Mech. Sci., 17, 813–823, 2026
https://doi.org/10.5194/ms-17-813-2026

Mechanical Sciences
Open Access

Research on reconfigurable kinematic analysis and type synthesis of planar prismatic Rubik's cube mechanism

Dabao Fan[1], **Daxing Zeng**[2], **Yuming Zhao**[1], **Haibing Feng**[1], **Yunjiao Deng**[2], **and Ya Liu**[2]

[1]College of mechanical and electrical engineering, Suqian University, Suqian 223800, P.R. China
[2]School of Mechanical Engineering, Dongguan University of Technology, Dongguan 523808, P.R. China

Correspondence: Dabao Fan (dabaofan@squ.edu.cn)

Received: 18 March 2026 – Revised: 15 July 2026 – Accepted: 15 July 2026 – Published: 17 August 2026

Abstract. A planar prismatic Rubik's cube mechanism (PPRCM) is defined as a Rubik's-cube-inspired mechanism whose rigid components are constrained to pure planar movements. Taking a typical PPRCM prototype as the research carrier, this paper elaborates on the composition, topological configuration, and reconfigurable motion process of the mechanism. The influencing factors of PPRCM's topological structure are abstracted, and the conditions for realizing reconfigurable motion are thereby derived. Based on the reconfigurable topological characteristics of PPRCM, a type synthesis method for the mechanism is proposed. By specifying the values of the topological influencing factors, PPRCMs with different topological structures are generated, and corresponding three-dimensional(3D) models are constructed to validate the rationality and effectiveness of the proposed method. The type synthesis method for PPRCM proposed in this paper not only enables the development of more novel PPRCM configurations but also enriches and improves the type synthesis theories for planar mechanisms.

1 Introduction

Compared with spatial mechanisms, planar mechanisms possess simple structural layouts that simplify theoretical derivation and numerical calculation, and they have a broad range of engineering application prospects. Similarly, spatial rotational Rubik's cube mechanisms adopt intricate spatial axis layouts and intersecting contact surfaces of revolute pairs (Fan et al., 2022). In contrast, all motions of planar Rubik's cube mechanisms are confined to a single plane, which brings about the merit of easy actuation. Meanwhile, planar Rubik's cube mechanisms also embody fascinating operational mechanisms. For instance, the eight-digit puzzle is a numerical game in which researchers rearrange eight numbered blocks in a 3×3 grid through moving operations. Scholars have carried out systematic research on its permutation rules and topological transformation laws. The most classic 3×3 Rubik's cube was invented by Ernő Rubik in 1974. Benefiting from its compact configuration and capacity to generate massive combinatorial configurations through basic movements, it has drawn extensive attention from both academia and the general public. Although the Rubik's cube was invented by Ernő Rubik, the core inspirations and concepts similar to it had long inspired the working people of ancient China. For example, Luo Shu is an ancient Chinese symbolic numerical pattern that inherently features the concept of transformation and rearrangement, a principle later reflected in Rubik's cubes. Luo Shu was employed to study weather, agriculture, solar terms, and other fields, ultimately promoting the development of production and daily life. After long-term inheritance and evolution, multiple derivative patterns derived from Luo Shu have been developed (Zeng et al., 2018). Later, mathematical games such as Magic Squares and the Backgammon appeared. The Backgammon consists of a 4×4 grid and 15 numbered tiles. The numbers 14 and 15 are swapped and misplaced in the initial state, and users can recover the standard arrangement by translating the number tiles.

The Rubik's cube offers entertainment and playability due to its vast number of combinatorial states, indicating that it inherently involves numerous important mathematical problems. Zassenhaus (1982) investigated group-theory-related issues in the Rubik's cube, such as subgroups, generators, and orders. Subsequently, Joyner (2008) extended the group-theoretic analysis of the Rubik's cube. Krutský and Šír (2025) introduced a novel symmetry-invariant neural architecture based on the rich symmetries and combinatorial properties of the Rubik's cube group. Mahindra Roshan et al. (2024) developed a deep-reinforcement learning approach for the combinatorial puzzle of the Rubik's cube, which learns to solve increasingly difficult states in reverse from the goal state.

Taking advantage of its property of massive combinatorial configurations, the Rubik's cube can also find application in the field of image encryption. The Rubik's cube, with an astronomical number of possible configurations, serves as an ideal encryption tool, and the combinatorial complexity of Rubik's cube, as well as other n-dimensional hypercubes, further opens up promising applications in cryptography, boasting significant potential for defense and other fields (Balasubramanian, 2024). Helmy et al. (2023) put forward a hybrid encryption architecture based on Rubik's cube theory to realize efficient encryption of facial, iris, and fingerprint biometric templates. Lai et al. (2020) leveraged the compact structural feature of the 3×3 Rubik's cube to design a modular Rubik's-cube-based microfluidic system, providing a promising solution to the problems of high cost and long processing time in the fabrication of microfluidic systems. Peng (2024) presented a Rubik's-cube-inspired educational tool in order to improve engineering ethics education and enhance lesson planning and assessment. Zhang et al. (2026) proposed a novel Rubik's-cube-inspired origami structure addressing spacecraft spatial needs, integrating electromagnetic and fluid functions. As a special type of reconfigurable mechanism, the planar prismatic Rubik's cube mechanism (PPRCM) realizes reconfiguration, topological variation, and structural deformation in a two-dimensional plane. It greatly simplifies the cognitive and analytical difficulty of complex reconfigurable mechanisms and lays a fundamental foundation for the subsequent extension to three-dimensional spatial mechanisms. Such variable and reconfigurable characteristics can be integrated with various engineering fields to produce cross-disciplinary research achievements. Over the last 5 decades, abundant research outcomes on Rubik's cube mechanisms have fully verified their research significance in modern multidisciplinary systems. Existing studies have proven that Rubik's cube mechanisms can be combined well with origami structures (Sharma et al., 2026), spatially deployable structures (Liu et al., 2022), and modular robots (Duan et al., 2026). In fact, Rubik's-cube-inspired design principles are applicable to almost all variable working scenarios, which can fully tap the application potential of Rubik's cube mechanisms in the field of deformable and reconfigurable equipment. Diversified novel Rubik's cube mechanisms can provide significant guidance for the innovative development of various disciplines. Accordingly, it is of great necessity to investigate the type synthesis method of the PPRCM.

Any movable system with definite motion can be regarded to be a mechanism. Therefore, such movable systems can be investigated from the perspective of mechanism theory. The PPRCM falls within the category of planar mechanisms, and existing theories on the type synthesis of planar mechanisms have become increasingly sophisticated. Historically, the synthesis of planar mechanisms originated from designers' experience and intuition. Subsequently, the synthesis of planar linkage mechanisms has evolved significantly, giving rise to a wealth of methods and theories. Davies and Crossley (1966) introduced a symbolic notation to represent plane pin-jointed kinematic chains and found all possible permutations of articulation for the purposes of censuses of 7-, 9-, 10-, and 11-bar chains. Tuttle et al. (1989) described a technique for enumerating all basic kinematic chains possessing N links and F degrees of freedom based on the theory of finite groups. Mruthyunjaya (1979) proposed a modified method of structural synthesis of linkage systems with positive, zero, or negative degrees of freedom by using the transformation of binary chains. Cao and Chu (1992) further developed the synthesis method based on the Assur group and synthesized all of the structural types of bar groups with multiple hinges up to eight bars with multiple hinges. Li et al. (2015) developed a new structural synthesis method by integrating Assur groups as elements in the newly developed group-based adjacency matrix. Slaboch and Voglewede (2011) represented the topological characteristics of reconfigurable mechanisms through the mechanism state matrices. Chan (2024) proposed a criterion for analyzing and synthesizing planar overconstrained mechanisms and obtained a systematic approach for synthesizing novel function cognates. Kong (2022) presented a method for the motion–structure mode analysis of n-RR planar parallelogram mechanisms. Santiago-Valentín et al. (2019) introduced the Santiago–Portilla method for representing any type of planar mechanisms independently of the number of elements or the link type. Huang et al. (2022) presented a computer-aided method to synthesize all feasible non-isomorphic mechanisms with one multiple-joint from the corresponding kinematic chains with one multiple-joint. Kang and Kim (2018) proposed a gradient-based topology optimization method to determine simultaneously the topology and joint type of planar linkage mechanisms. Deng and Purwar (2024) introduced a novel matrix-based approach for the simultaneous type and dimensional synthesis of planar four-bar linkage mechanisms. Vinícius Morlin et al. (2024) investigated the type synthesis of non-redundant planar kinematic chains applied to parallel mechanisms. Yim et al. (2021) proposed a neural-network-based big-data approach to simultaneously determine the mechanism topology and its end-effector location. The planar one-rotational one-translational and one-rotational two-translational parallel mechanisms that evolved from the crank-and-rocker mechanism are presented by means of Lie group theory (Jin et al., 2018). Ye et al. (2014) studied the characteristics of planar five-bar metamorphic linkages, and four kinds of planar five-bar metamorphic linkages were enumerated. Zhang et al. (2021) proposed a limb-constraint-based synthesis method that matches structural chains with the prescribed output motion of the moving platform. Liu et al. (2023) obtained a planar rhombus 4R mechanism by adding two or four revolute joints to a planar rhombus 4R mechanism, and then reconfigurable single-loop mechanisms were synthesized. Although mature type synthesis theories for planar linkages have been well established, due to the unique characteristics of Rubik's cube mechanisms, these methods are hardly applicable to the type synthesis design of the PPRCM.

Whether it is numerical puzzle games such as Magic Squares, the eight-digit puzzle, and the Backgammon or casual games like Klotski game, all of them achieve the final target state by moving blocks within a plane. Their essence lies in planar mechanisms with prismatic pairs. To obtain more PPRCMs with diverse topological structures, expand the types of PPRCM, and enrich products centered on PPRCM, this paper investigates the reconfigurable motion of PPRCM and proposes a type synthesis method for the PPRCM. Section 2 thoroughly illustrates the internal structure and reconfigurable motion process of the PPRCM. Section 3 provides a rigorous definition and analysis of the prismatic-pair contact surface(PPCS). Section 4 derives the constraint criteria for realizing PPRCM reconfiguration motion. Section 5 puts forward the type synthesis method for the PPRCM. Section 6 presents specific type synthesis cases and obtains PPRCMs with specific topological structures. Finally, the conclusions are drawn in Sect. 7.

2 Introduction of the PPRCM

Next, taking the PPRCM prototype illustrated in Fig. 1 as a research case, we elaborate upon the structural composition. Figure 2 presents the corresponding 3D printed model. This PPRCM mainly consists of two parts, including a base and moving modules. The moving modules include moving module M_1, moving module M_2, and moving module M_3. The base features uniformly distributed grooves along the X_0 and Y_0 directions, which can dynamically connect the moving modules, allowing them to achieve translational movement along their respective grooves, as illustrated in Fig. 3. This design draws inspiration from the classic ancient Chinese tenon-and-mortise joint structure. The moving grooves serve as the moving paths. The moving modules can perform translational movements on the base along the X_0 and Y_0 directions, denoted as moving directions ${}^0K_2$ and ${}^0K_1$, respectively. Six paths are evenly distributed along the X_0 direction, including ${}^0T_{j1}^{{}^0K_2}$, ${}^0T_{j2}^{{}^0K_2}$, ${}^0T_{j3}^{{}^0K_2}$, ${}^0T_{j4}^{{}^0K_2}$, ${}^0T_{j5}^{{}^0K_2}$, and ${}^0T_{j6}^{{}^0K_2}$. Similarly, six paths are evenly distributed along the Y_0 direction, including ${}^0T_{j1}^{{}^0K_1}$, ${}^0T_{j2}^{{}^0K_1}$, ${}^0T_{j3}^{{}^0K_1}$, ${}^0T_{j4}^{{}^0K_1}$, ${}^0T_{j5}^{{}^0K_1}$, and ${}^0T_{j6}^{{}^0K_1}$.

Three distinct motion modes are available for the PPRCM presented in Fig. 1. Firstly, the moving module translates along the Y_0 direction; secondly, the moving module translates along the X_0 direction; thirdly, the moving block translates along the X_0 direction on the moving-block side piece (MBSP). The moving block consists of a moving block and MBSPs. The MBSPs are equipped with clamping pins, which ensure that the MBSPs are engaged in the grooves of the base when moving along the X_0 and Y_0 directions. Meanwhile, the MBSPs are provided with grooves that allow the moving block to be locked onto them during movement along the X_0 direction, as shown in Fig. 4. The contact region between the MBSPs and the base is square-shaped, enabling the moving module to move within the range of the PPRCM base along the X_0 and Y_0 directions (i.e., the first and second movement mode). In practice, the moving block is "attached" to the MBSPs during these scenarios, meaning the

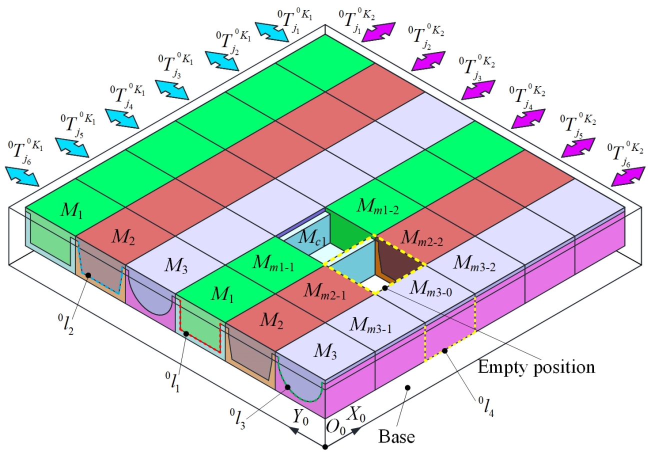

Figure 1. The three-dimensional model diagram of the PPRCM.

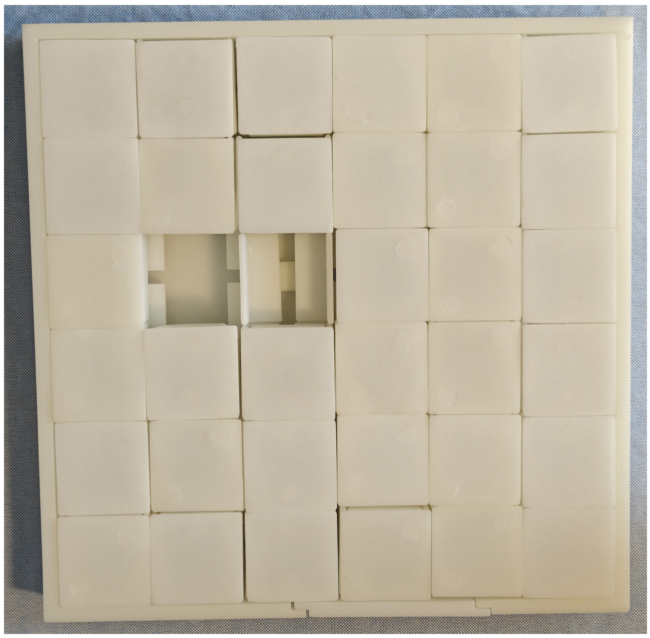

Figure 2. Schematic diagram of 3D-printed model for PPRCM.

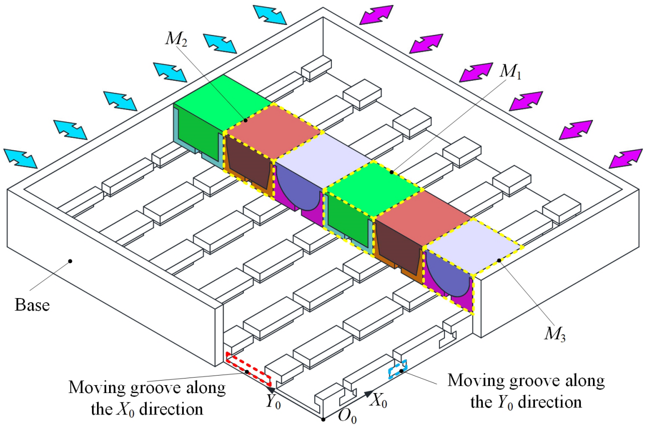

Figure 3. Schematic diagram of the internal structure of the PPRCM.

movement of the moving module is essentially the movement of the MBSPs. Each MBSP occupies a specific "position" on the base, and a vacant unoccupied slot is defined as an "empty position". For the third movement mode, the contact interface between the moving block and the MBSP serves as the prismatic-pair contact surface, and the intersection of the plane perpendicular to the movement direction with this contact surface forms the profile of the prismatic-pair contact surface for that direction. Since the prismatic-pair contact surfaces are identical for the first two scenarios but differ in the third, this provides more configuration possibilities for PPRCM design. Accordingly, the third motion mode is chosen as the core research object for the subsequent theoretical derivation and analysis.

To intuitively and clearly visualize the prismatic-pair contact surfaces and their corresponding profiles, the PPRCM is simplified as illustrated in Fig. 1. Subsequently, the internal structure of all PPRCMs discussed hereafter can be referenced to the PPRCM shown in Fig. 3.

Since the PPRCM only involves translational motion, at least one empty position is required to realize its reconfiguration capability. Furthermore, this paper mainly targets the third motion mode; it is necessary that only one MBSP M_{C1} occupies a single position, as shown in Fig. 1. In the third scenario, since the moving module translates along the X_0 direction on the MBSP, there must be adjacent MBSP in the direction of the moving block's movement. As depicted in Fig. 1, the moving blocks M_{m2-1} and M_{m2-2} cannot move along the X_0 direction because there are no adjacent MBSPs in their X_0 direction. In contrast, the moving blocks M_{m1-1} and M_{m1-2} can move along the X_0 direction as these two modules have an adjacent MBSP M_{C1} in the X_0 direction.

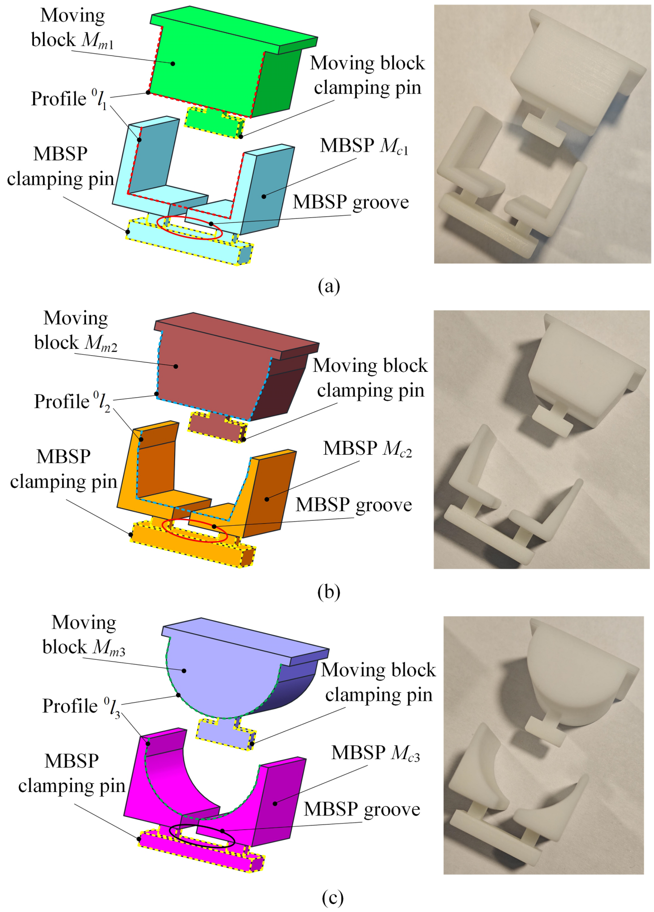

Figure 4. Schematic diagrams of the three-dimensional models and 3D-printed prototypes of different moving module for the PPRCM. **(a)** Moving module M_1. **(b)** Moving module M_2. **(c)** Moving module M_3.

3 Description and analysis of PPCS

The PPRCM only contains prismatic kinematic pairs with diversified structural forms. To facilitate the analysis and design of PPRCM, a parametric representation of the PPCS is first established. A prismatic pair refers to a movable connection between two components with relative linear motion, serving as a constraint that provides only 1 translational degree of freedom. As illustrated in Fig. 5a, the moving component translates relative to the fixed component along the moving direction z_1, and the direct contact area between the two components forms the PPCS. A plane that is perpendicular to the moving direction and capable of sectioning both the fixed component and the moving component simultaneously is defined as the cross-sectional plane. The intersection line formed by this cross-sectional plane and the PPCS is the profile l_1 of the PPCS.

Next, a parametric description of the prismatic pair is performed. A Cartesian coordinate system o_1-$x_1y_1z_1$ is constructed, as illustrated in Fig. 5, where the cross-sectional

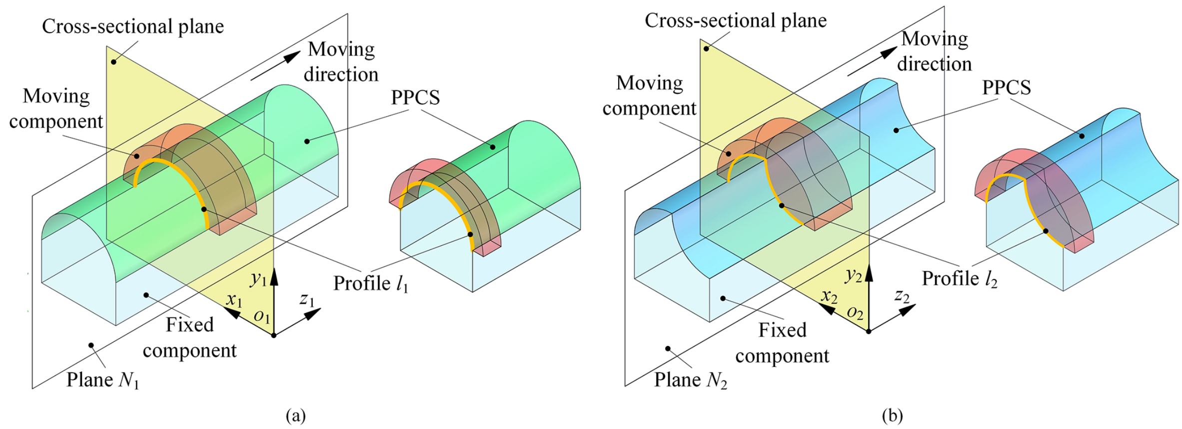

Figure 5. Schematic diagram of the PPCS. **(a)** Symmetric PPCS. **(b)** Asymmetric PPCS.

plane serves as the o_1-x_1y_1 plane and where the translational direction of the movable component is taken as the z_1 axis. Since the PPCS is a curved surface formed by extruding the profile l_1 along the moving direction, it can be uniquely determined under the coordinate system o_1-$x_1y_1z_1$ through the profile l_1. Furthermore, as the profile of the PPCS lies entirely inside the o_1-x_1y_1 plane of the coordinate system, it is expressed by the equation $f_1(x_1, y_1) = 0$. Additionally, when multiple PPCSs of different types exist in a single coordinate system, the parametric representations of all PPCSs can be obtained using the above-mentioned modeling approach.

In addition, owing to diversified reconfiguration motions, PPCSs can take different forms, as illustrated by the two distinct types shown in Fig. 5. A PPCS is classified as symmetric if there exists a plane parallel to the moving direction, with respect to which the PPCS is symmetric. Conversely, a PPCS is deemed to be asymmetric if no such plane parallel to the moving direction can be found to satisfy the symmetry condition. Specifically, as illustrated in Fig. 5a, there exists a plane N_1 parallel to the moving direction, with respect to which the corresponding PPCS is symmetric; hence, this PPCS is categorized as symmetric. As shown in Fig. 5b, however, no plane N_2 parallel to the moving direction can be identified to achieve symmetry for the relevant PPCS. Therefore, this PPCS should be defined as asymmetric. For simplicity, only symmetric PPCSs are adopted for all subsequent theoretical analyses in this paper.

4 Conditions for realizing reconfigurable motion of the PPRCM

For the components in the PPRCM to interchange positions and achieve reconfigurable motion, the following conditions must be satisfied.

1. *Identical movement slopes.*

   The movement slope refers to the moving direction. In the same PPRCM, only components sharing identical translational axes are mutually interchangeable. Component interchange occurs between parts located on different moving paths but with the same moving direction, thereby enabling reconfigurable motion. When moving directions are inconsistent, components do not exhibit identical motion behaviors.

2. *The PPCS shall satisfy the inclusivity requirement.*

   When moving directions are identical, components are capable of moving along different moving paths within the same direction. However, given that different moving paths in the same direction may be associated with distinct PPCSs, it is necessary to analyze the inclusivity of these PPCSs. Since a PPCS can be uniquely defined by its corresponding profile, the inclusivity of PPCSs can be analyzed by comparing the profile corresponding to the PPCS on different moving paths in the same direction.

   Taking the PPRCM illustrated in Fig. 1 as a research case, the movement operation along the X_0 direction is selected for analysis. Therefore, the three profiles corresponding to the X_0 direction are selected for the inclusivity analysis of PPCSs in the subsequent part. The PPCSs formed between the moving block and MBSP inside the three moving modules can be represented by the respective profiles. To facilitate the follow-up theoretical comparison, the three profiles ${}^0l_1$, ${}^0l_2$, and ${}^0l_3$ are compared and analyzed together, as shown in Fig. 6.

   For any given x, if the corresponding function values $f_1(x)$ and $f_2(x)$ on the two different profiles l_1 and l_2 satisfy $f_1(x) \leq f_2(x)$ then profile l_2 is said to be contained in profile l_1, or profile l_1 contains profile l_2, denoted as $l_1 \supseteq l_2$ or $l_2 \subseteq l_1$. In Fig. 6, profile ${}^0l_1$ contains profile ${}^0l_2$, profile ${}^0l_2$ contains profile ${}^0l_3$, and it is obvious that profile ${}^0l_1$ contains profile ${}^0l_3$. This is the transitivity of profile inclusivity, denoted as follows: if ${}^0l_1 \supseteq {}^0l_2$ and ${}^0l_2 \supseteq {}^0l_3$ then ${}^0l_1 \supseteq {}^0l_3$. Or, if ${}^0l_2 \subseteq {}^0l_1$ and

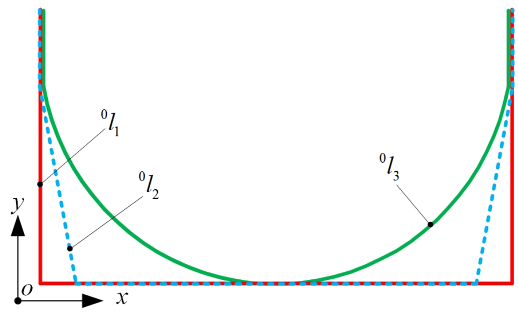

Figure 6. Schematic diagram of moving-block profile comparison.

$^0l_3 \subseteq {}^0l_2$ then $^0l_3 \subseteq {}^0l_1$. In this case, the moving component corresponding to profile $^0l_2$ can move on the fixed component corresponding to profile $^0l_1$.

This section intercepts a local segment of the PPRCM prototype in Fig. 1 to derive the configuration displayed in Fig. 7a. The MBSP M_{c1} translates along the negative Y_0 to reach the configuration in Fig. 7b. Under this layout, the moving block M_{m2} can slide along the negative X_0 to reach the state shown in Fig. 7c, which is because profile $^0l_1$ contains profile $^0l_2$. A part of the PPRCM shown in Fig. 1 is selected to get the state presented in Fig. 8a. The MBSP M_{c3} moves along the Y_0 direction to obtain the state shown in Fig. 8b. At this moment, the moving block M_{m2} cannot move along the reverse direction of X_0 to the MBSP M_{c3} shown in Fig. 8b; this is because profile $^0l_2$ contains profile $^0l_3$.

3. *At least two different intersecting slopes exist.*

   All motions of the PPRCM take place in a planar space, and two different movement slopes indicate two distinct moving directions, which in turn lead to the generation of intersecting components. If only one movement slope exists, all movements are parallel to each other, and no intersecting components will be generated. In this case, there will be no components capable of moving along two directions, making it impossible to realize reconfigurable motion. Accordingly, the PPRCM must contain at least two mutually intersecting moving directions.

5 Type synthesis method of the PPRCM

Based on the above analysis of the conditions for realizing reconfigurable motion of the PPRCM, a type synthesis method for PPRCM is proposed as follows:

1. Determine the moving direction number K_i in the PPRCM, namely the number of movement slope K_i ($i = 1, 2, \ldots, n$). Since the movement is linear within a plane, the moving directions of the PPRCM can be regarded as straight lines in the plane coordinate system. Different moving paths under the same moving direction are parallel straight lines, and different moving directions are straight lines with different slopes. Theoretically, here, the movement slopes can be arbitrarily assigned. In the PPRCM illustrated in Fig. 1, the number of moving directions is 2 along the Y_0 direction and X_0 direction, denoted as $^0K_2$ and $^0K_1$, respectively.
2. Determine the number $j\,(j \geq 2)$ of moving path $T_j^{K_i}$ in the moving direction K_i; specifically, define the moving paths $T_1^{K_i}, T_2^{K_i}, \ldots, T_j^{K_i}$ in the moving direction K_i. In the PPRCM illustrated in Fig. 1, the number of moving paths j in the moving direction $^0K_1$ is six, denoted as $^0T_{j1}^{^0K_1}$, $^0T_{j2}^{^0K_1}$, $^0T_{j3}^{^0K_1}$, $^0T_{j4}^{^0K_1}$, $^0T_{j5}^{^0K_1}$, and $^0T_{j6}^{^0K_1}$; the number of moving paths j in the moving direction $^0K_2$ is six, denoted as $^0T_{j1}^{^0K_2}$, $^0T_{j2}^{^0K_2}$, $^0T_{j3}^{^0K_2}$, $^0T_{j4}^{^0K_2}$, $^0T_{j5}^{^0K_2}$, and $^0T_{j6}^{^0K_2}$.
3. Determine the types of PPCSs in the moving direction K_i. In the PPRCM illustrated in Fig. 1, the six PPCSs in the moving direction $^0K_1$ are identical; the six PPCSs in the moving direction $^0K_2$ can be categorized into three types, and the profiles of these PPCSs are shown in Fig. 6. According to the previous analysis on the inclusivity requirement, it can be concluded that $^0l_3 \subseteq {}^0l_2 \subseteq {}^0l_1$.
4. Determine the base such that all movable components can be placed on the base to perform movement operations.

The procedural steps of the above-mentioned type synthesis method are summarized in Fig. 9.

6 Type synthesis case of PPRCM

Through the analysis of the reconfigurable motion of the PPRCM, the factors affecting the topological structure of the PPRCM can be obtained, including the number K_i of movement slopes ($i = 1, 2, \ldots, n$), the number j of moving paths in the moving direction K_i, and the types of PPCSs in the moving direction K_i. Next, different topological structures of the PPRCM can be obtained by specifying each of these factors.

6.1 The number K_i of different movement slopes

The number of movement slopes directly determines the topological structure of the PPRCM. The higher the number of movement slopes, the more interchangeable components the PPRCM contains. By configuring different movement slopes, we obtain the configurations shown in Fig. 10: two movement slopes in Fig. 10a and b, three movement slopes in Fig. 10c, and four movement slopes in Fig. 10d. Among them, in Fig. 10a, the moving directions $^1K_1$ and $^1K_2$ are along the Y_1 direction and X_1 direction, respectively. In

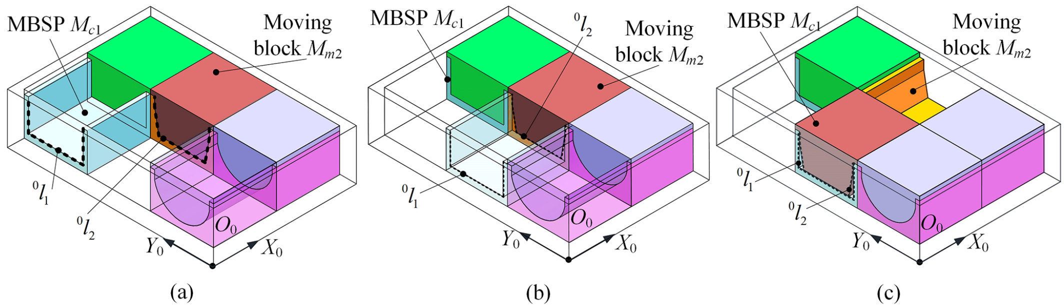

Figure 7. Schematic diagram of the moving component corresponding to the profile $^0l_2$ moving on the fixed component corresponding to the profile $^0l_1$. **(a)** State 1. **(b)** State 2. **(c)** State 3.

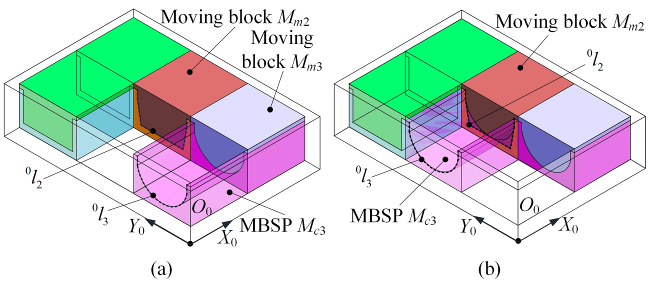

Figure 8. Schematic diagram of the moving component corresponding to the profile $^0l_2$ that is not able to move on the fixed component corresponding to the profile $^0l_3$. **(a)** State 1. **(b)** State 2.

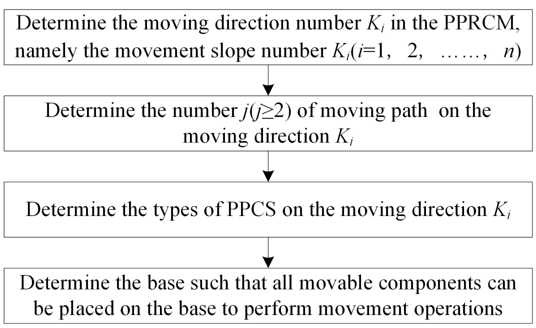

Figure 9. Type synthesis method of the PPRCM.

Fig. 10b, the moving direction $^2K_1$ is along the Y_2 direction, and the moving direction $^2K_2$ forms a 45° with the positive direction of X_2 (counterclockwise rotation is defined as the positive angular direction). In Fig. 10c, the moving directions $^3K_1$, $^3K_2$, and $^3K_3$ are along the Y_3 direction, X_3 direction, and a 45° with the positive direction of X_3, respectively. In Fig. 10d, the moving directions $^4K_1$, $^4K_2$, $^4K_3$, and $^4K_4$ are along the Y_4 direction, X_4 direction, a 45° with the positive direction of X_4, and a −45° with the positive direction of X_4, respectively. All subgraphs adopt reference coordinate systems with identical orientation, and only the coordinate symbols are distinguished for labeling.

6.2 The number of moving paths $T_{j_i}^{K_i}$ in the moving direction K_i

In the PPRCM, after determining the movement slopes, it is necessary to specify the number of moving paths corresponding to each movement slope. For example, in Fig. 11a, the moving directions $^5K_2$ and $^5K_1$ are along the X_5 direction and Y_5 direction, respectively; in Fig. 11b, the moving direction $^6K_1$ is along the Y_6 direction, and the moving direction $^6K_2$ forms a 45° with the positive direction of X_6. Each movement slope in Fig. 1 has six moving paths, each movement slope in Fig. 10a has four moving paths, and each movement slope in Fig. 11a has three moving paths. The PPRCMs shown in Figs. 10b and 11b have two non-orthogonal movement slopes. For the PPRCM in Fig. 10b, there are four moving paths on the movement slope $^2K_1$ and three moving paths on the movement slope $^2K_2$. For the PPRCM in Fig. 11b, there are three moving paths on both the movement slope $^6K_1$ and the movement slope $^6K_2$.

6.3 The types of PPCSs in the moving direction

When the number K_i of movement slopes ($i = 1, 2, \ldots, n$) and the number of moving paths on each moving direction K_i are the same, PPRCM with different topological structures can be obtained by changing the types of PPCSs in the moving direction K_i, as illustrated in Fig. 12, with the corresponding profiles shown in Fig. 13. In Fig. 12a, the moving directions $^7K_2$ and $^7K_1$ are along the X_7 direction and Y_7 direction, respectively, and the inclusivity of PPCSs can be represented by $^7l_1\subset{}^7l_2\not\subset{}^7l_3\subset{}^7l_4$. In Fig. 12b, the moving directions $^8K_2$ and $^8K_1$ are along the X_8 direction and Y_8 direction, respectively, and the inclusivity of PPCSs can be represented by $^8l_1\subset{}^8l_2\subset{}^8l_3\subset{}^8l_4 \subset$. In Fig. 12c, the moving directions $^9K_2$ and $^9K_1$ are along the X_9 direction and Y_9 direction, respectively, and the inclusivity of PPCS can be represented by $^9l_1\subset{}^9l_2\not\subset{}^9l_3\subset{}^9l_4$. In Fig. 12d, the moving directions $^{10}K_2$ and $^{10}K_1$ are along the X_{10} direction and Y_{10} direction, respectively, and the inclusivity of PPCS can be represented by $^{10}l_1\not\subset{}^{10}l_2\not\subset{}^{10}l_3\subset{}^{10}l_4$. The reconfigurable

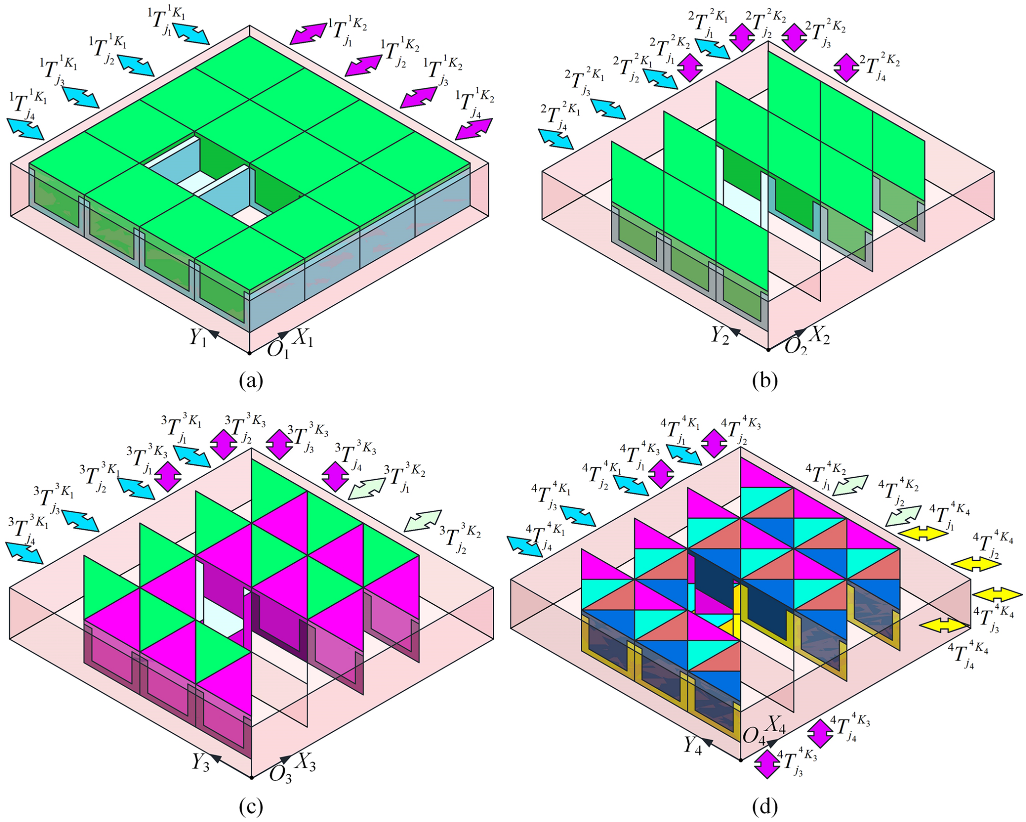

Figure 10. Schematic diagram of PPRCM with different numbers of movement slopes.

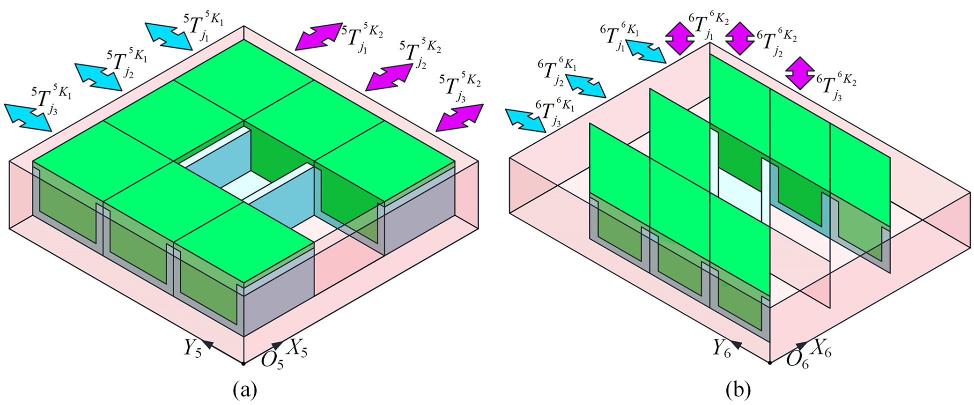

Figure 11. Schematic of the PPRCM with varying moving-path counts per direction.

motion characteristics of the PPRCM can be derived based on the analysis presented in Sect. 4.

7 Conclusions

This paper conducts a comprehensive analysis of the structural composition, topological configuration, and reconfigurable motion process of the PPRCM. Three factors that dominate the topological characteristics of the PPRCM are summarized, and the essential constraint criteria for achieving its reconfigurable motion are derived. A type synthesis method for the PPRCM is proposed, with specific synthesis steps given. By assigning values to the topological structure-influencing factors, PPRCMs with different topological structures are synthesized, and corresponding 3D prototype models are established, verifying the correctness of the proposed type synthesis method. The type synthesis method for the PPRCM proposed in this work can offer valuable theoretical references for relevant research on planar mechanisms and reconfigurable mechanisms.

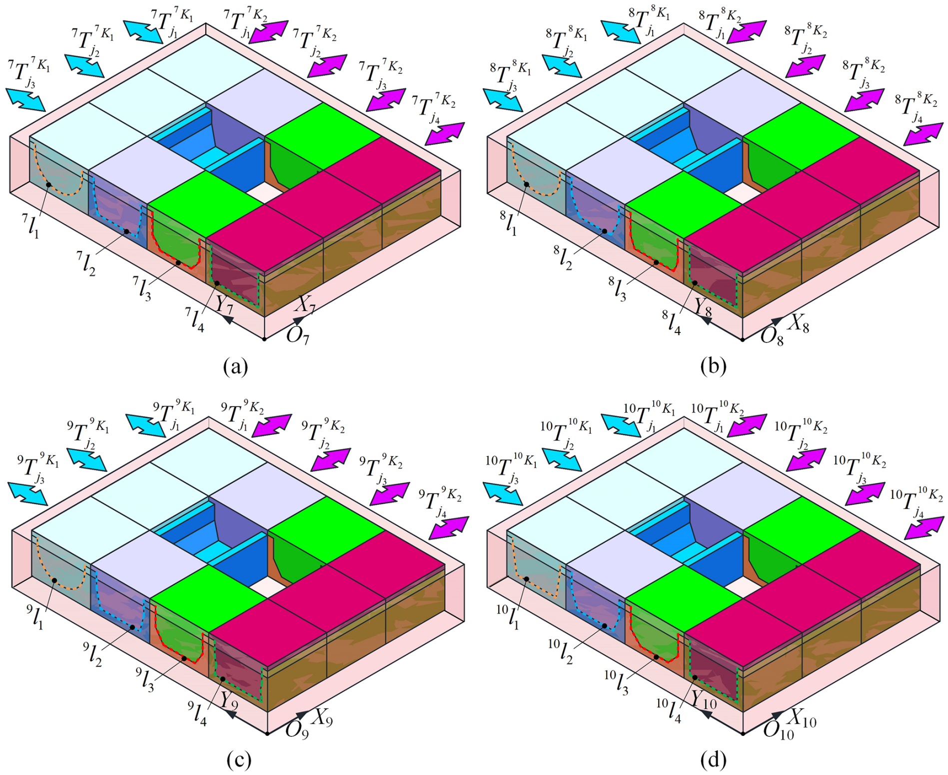

Figure 12. Schematic diagram of different types of PPCSs.

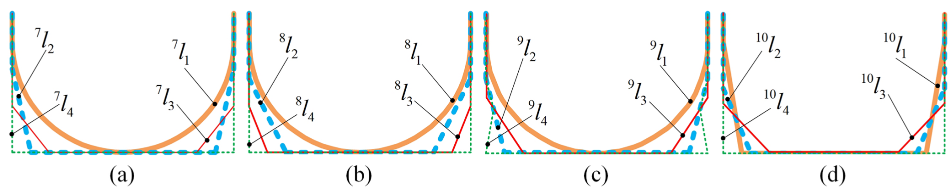

Figure 13. Schematic diagram of profiles of different types of PPCSs.

Data availability. The data used in this study are not publicly available due to laboratory confidentiality requirements. Relevant information may be made available by the corresponding author upon reasonable request and with permission from the laboratory.

Author contributions. Dabao Fan and Daxing Zeng proposed the research design and framework of the paper. Dabao Fan drafted the initial paper draft. Yuming Zhao drew the model. Haibing Feng reviewed the entire paper and provided guidance for the revisions. Yunjiao Deng and Ya Liu contributed to the literature review and model construction.

Competing interests. The contact author has declared that none of the authors has any competing interests.

Disclaimer. Publisher's note: Copernicus Publications remains neutral with regard to jurisdictional claims made in the text, published maps, institutional affiliations, or any other geographical representation in this paper. The authors bear the ultimate responsibility for providing appropriate place names. Views expressed in the text are those of the authors and do not necessarily reflect the views of the publisher.

Acknowledgements. This work was supported by Jiangsu Engineering Research Center of Key Technology for Intelligent Manufacturing Equipment, China.

Financial support. This research has been supported by the Scientific Research Foundation for the Introduction of Talents, Sugian University (grant no. 2025XRC039) and Guangdong Basic and Applied Basic Research Foundation (grant no. 2025A1515110340).

Review statement. This paper was edited by Pengyuan Zhao and reviewed by two anonymous referees.

References

Balasubramanian, K.: Enumeration of n-dimensional hyper-cubes, icosahedra, rubik's cube dice, colorings, chirality, and encryptions based on their symmetries, Symmetry, 16, 1020, https://doi.org/10.3390/sym16081020, 2024.

Cao, W. Q. and Chu, J. K.: Synthesis of assur groups with multiple joints, Mech. Mach. Theory, 5, 24–27, https://doi.org/10.1016/S0094-114X(97)00117-1, 1992.

Chan, C. L.: A general method to synthesize planar overconstrained mechanism, Mech. Mach. Theory, 203, 105801, https://doi.org/10.1016/j.mechmachtheory.2024.105801, 2024.

Davies, T. H. and Crossley, F. R. E: Structural analysis of plane linkages by Franke's condensed notation, J. Mech., 1, 171–183, https://doi.org/10.1016/0022-2569(66)90021-8, 1966.

Deng, X. and Purwar, A.: A matrix-based approach to unified synthesis of planar four-bar mechanisms for motion generation with position, velocity, and acceleration constraints, J. Comput. Inf. Sci. Eng., 24, 121003, https://doi.org/10.1115/detc2024-143028, 2024.

Duan, Q. C., Sun, J. L., and Hu, H. Y.: Dynamic analysis and experiments on the assembly control of planar deployable modules, Space-Sci. Tech.-China, 0648, https://doi.org/10.34133/space.0648, 2026.

Fan, D. B., Zeng, D. X., Liu, Y., Lu, W. J., Hou, Y. L., Zhou, Z. R., and Guo, J. W.: Topological structure of Rubik's cube mechanism and synthesis of the regular hexahedron Rubik's cube mechanism, J. Mech. Sci. Technol., 36, 1935–1947, https://doi.org/10.1007/s12206-022-0330-4, 2022.

Helmy, M., ElRabaie, E. S. M., ElDokany, I., and Abd ElSamie, F. E.: A novel cancellable biometric recognition system based on Rubik's cube technique for cyber-security applications, Optik, 285, 170475, https://doi.org/10.1016/j.ijleo.2022.170475, 2023.

Huang, P., Liu, T. T., Ding, H. F., and Zhao, Y.: Computer-aided synthesis of planar mechanisms with one multiple-joint, Mech. Mach. Theory, 177, 105044, https://doi.org/10.1016/j.mechmachtheory.2022.105044, 2022.

Jin, X. D., Fang, Y. F., Guo, S., and Qu, H. B.: Structural synthesis of parallel mechanisms with high rotational capability, Chin. J. Mech. Eng-En., 31, 61, https://doi.org/10.1186/s10033-018-0260-3, 2018.

Joyner, D.: Adventures in group theory: rubik's cube, merlin's machine, and other mathematical toys, The Johns Hopkins University Press, Baltimore, America, Maryland, 167–198, ISBN 978-0801890130, 2008.

Kang, S. W. and Kim, Y. Y.: Unified topology and joint types optimization of general planar linkage mechanisms, Struct. Multidiscip. O., 57, 1955–1983, https://doi.org/10.1007/s00158-017-1887-x, 2018.

Kong, X. W.: Motion/structure mode analysis and classification of n-RR planar parallelogram mechanisms, Mech. Mach. Theory, 169, 104623, https://doi.org/10.1016/j.mechmachtheory.2021.104623, 2022.

Krutský, M. and Šír, G.: Geometric deep learning for the Rubik's cube group, IEEE. T. Neur. Net. Lear., 36, 20214–20228, https://doi.org/10.1109/TNNLS.2025.3599009, 2025.

Lai, X. C., Shi, Z., Pu, Z. H., Zhao, P. H., Zhang, X. G., Yu, H. X., and Li, D. C.: A Rubik's microfluidic cube, Microsyst. Nanoeng., 6, 27, https://doi.org/10.1038/s41378-020-0136-4, 2020.

Li, S. J., Wang, H. G., and Dai, J. S.: Assur-group inferred structural synthesis for planar mechanisms, J. Mech. Robot., 7, 041001, https://doi.org/10.1115/1.4029116, 2015.

Liu, J. G., Zhao, P. Y., Chen, K. L., Zhang, X., and Zhang. X.: 1U-sized deployable space manipulator for future on-orbit servicing, assembly, and manufacturing, Space-Sci Tech-China, 2022, 9894604, https://doi.org/10.34133/2022/9894604, 2022.

Liu, Y., Yao, Y. A., Kong, X. W., and Li, Y. Z.: Type synthesis of reconfigurable single-loop mechanisms based on planar rhombus mechanisms, Mech. Mach. Theory, 181, 105170, https://doi.org/10.1016/j.mechmachtheory.2022.105170, 2023.

Mahindra Roshan, M., Rakesh, S., Sri Gnana Guru, T., Rohith, B., and Hemalatha, J.: Towards efficiently solving the rubik's cube with deep reinforcement learning and recursion, E3S Web Conf., 491, 01009, https://doi.org/10.1051/e3sconf/202449101009, 2024.

Mruthyunjaya, T. S.: Structural synthesis by transformation of binary chains, Mech. Mach. Theory, 14, 221–231, https://doi.org/10.1016/0094-114X(79)90009-0, 1979.

Peng, Y. Q.: A Rubik's cube-inspired pedagogical tool for teaching and learning engineering ethics, Sci. Eng. Ethics., 30, 50, https://doi.org/10.1007/s11948-024-00506-z, 2024.

Santiago-Valentín, E., Portilla-Flores, E. A., Mezura-Montes, E., Vega-Alvarado, E., Calva-Yáñez, M. B., and Pedroza-Villalba, M.: A graph-theory-based method for topological and dimensional representation of planar mechanisms as a computational tool for engineering design, IEEE Access, 7, 587–596, https://doi.org/10.1109/access.2018.2885563, 2019.

Sharma, A., Naskar, S., and Mukhopadhyay, T.: Programmable shape morphing and space deployment through graded derivatives of origami architectures, Space-Sci. Tech.-China, 6, 0363, https://doi.org/10.34133/space.0363, 2026.

Slaboch, B. J. and Voglewede, P. A.: Mechanism state matrices for planar reconfigurable mechanisms, J. Mech. Robot., 3, 11012, https://doi.org/10.1115/1.4003270, 2011.

Tuttle, E. R., Peterson, S. W., and Titus, J. E.: Enumeration of basic kinematic chains using the theory of finite groups, J. Mech. Transm.-T. ASME, 111, 498–503, 1989.

Vinícius Morlin, F., Piga Carboni, A., and Martins, D.: Structural synthesis of planar kinematic chains for non-redundant parallel manipulators, J. Mech. Design, 146, 113302, https://doi.org/10.1115/1.4065317, 2024.

Ye, W., Fang, Y. F., and Guo, S.: Reconfigurable parallel mechanisms with planar five-bar metamorphic linkages, Sci. China Technol. Sc., 57, 210–218, https://doi.org/10.1007/s11431-013-5433-9, 2014.

Yim, N. H., Lee, J., Kim, J., and Kim, Y. Y.: Big data approach for the simultaneous determination of the topology and end-effector location of a planar linkage mechanism, Mech. Mach. Theory, 163, 104375, https://doi.org/10.1016/j.mechmachtheory.2021.104375, 2021.

Zassenhaus, H.: Rubik's Cube: A Toy, A galois tool, group theory for everybody, Physica A., 114, 629–637, https://pascal-francis.inist.fr/vibad/index.php?action=getRecordDetail&idt=PASCAL83X0093914 (last access: 14 August 2026), 1982.

Zeng, D. X., Li, M., Wang, J. J., Hou, Y. L., Lu, W. J., and Huang, Z.: Overview of Rubik's cube and reflections on its application in mechanism, Chin. J. Mech. Eng-En., 31, 9–20, https://doi.org/10.1186/s10033-018-0269-7, 2018.

Zhang, D. S., Zheng, Y., Wei, L., Wu, J., Xu, Y. D., and Zhao, Y. S.: Type synthesis of 2T1R planar parallel mechanisms and their modeling development applications, IEEE Access, 9, 72217–72227, https://doi.org/10.1109/ACCESS.2021.3079266, 2021.

Zhang, J., Liu, S., Chen, J. T., and Wang, C. G.: Aerodynamic and electromagnetic analysis of a Rubik's cube-inspired origami structure, Aerosp. Sci. Technol., 168, 110979, https://doi.org/10.1016/j.ast.2025.110979, 2026.